



CHORUS

This is the accepted manuscript made available via CHORUS. The article has been published as:

Multiple-Wave Diffraction in High Energy Resolution Back-Reflecting X-Ray Optics

Yuri P. Stetsko, J. W. Keister, D. S. Coburn, C. N. Kodituwakku, A. Cunsolo, and Y. Q. Cai

Phys. Rev. Lett. **107**, 155503 — Published 7 October 2011

DOI: [10.1103/PhysRevLett.107.155503](https://doi.org/10.1103/PhysRevLett.107.155503)

Multiple-Wave Diffraction in High Energy-Resolution Back-Reflecting X-Ray Optics

Yuri P. Stetsko, J. W. Keister, D. S. Coburn, C. N. Kodituwakku, A. Cunsolo, and Y. Q. Cai*
National Synchrotron Light Source II, Brookhaven National Laboratory, Upton, New York 11973, USA
 (Dated: September 1, 2011)

We have studied the effects of multiple-wave diffraction (MWD) in a novel optical scheme recently published by Shvyd'ko et al. utilizing Bragg diffraction of x-rays in backscattering geometry from asymmetrically cut crystals for achieving energy resolutions beyond the intrinsic width of the Bragg reflection. By numerical simulations based on dynamic x-ray diffraction and by experimentation involving two-dimensional angular scans of the back-reflecting crystal, MWD was found to contribute up to several tens percents loss of efficiency but can be avoided without degrading the energy resolution of the original scheme by careful choice of azimuthal orientation of the diffracting crystal surface and by tilting of the crystal perpendicular to the dispersion plane.

PACS numbers: 61: 61.10-I, 41.50.+h, 42.25.Fx

Multiple-wave diffraction (MWD) is an important element of any x-ray optical scheme utilizing Bragg diffraction from high quality single crystals [1, 2]. On one hand, MWD extends the range of traditional two-wave x-ray optics to multiple-wave ones with unique properties and applications in high-resolution monochromators, interferometers, resonators, and spectrometers [2]. On the other hand, MWD can produce very strong parasitic effects, leading to loss of efficiency and degraded energy resolution of the x-ray optics [2]. Optical schemes with x-ray back reflections from perfect crystals of high crystallographic symmetry, such as single crystals of silicon and diamond, are particularly prone to such destructive effects as they are always accompanied by MWD with relatively large number of diffracted waves [1–6]. Therefore, analysis of MWD in x-ray back-reflecting optics, as well as the search for ways to minimize or to eliminate entirely its destructive contribution, is of practical importance for their applications and is the main goal of the present paper.

The novel optical scheme recently published by Shvyd'ko et al. [7] presents a unique case for analysis. It exploits the angular dispersion of x-ray back reflections from asymmetrically cut crystals for achieving energy resolutions beyond the limit set by the intrinsic width of the Bragg reflection in single symmetric back-reflecting crystal optics [8, 9]. An energy resolving power as high as 10^8 at a moderate energy of ~ 10 keV can be achieved by proper choice of the Bragg reflection and the asymmetry angle of the back-reflecting crystal [1]. The optical scheme includes three crystals: a Collimator (*C*), a Disperser (*D*), and a Selector (*S*) crystal (see Fig. 1 (a)). The *D* crystal is the backscattering crystal of the scheme at Si(800) reflection and sets the operation energy E at 9.1316 keV ($\theta_D^{Bragg} = 90^\circ$). For the present analysis, the asymmetry angle η_D is chosen to be 88° . The *C* crystal is a 200 μm thick Si(220) crystal with an asymmetry angle $\eta_C = 19^\circ$ designed to collimate the incident beam for incidence to the *D* crystal, and to provide a large angular acceptance of ~ 100 μrad for the optical scheme. X-

rays reflected by the *D* crystal disperse in angle according to their wavelength as a result of the angular dispersion effect [1], and then transmit through the *C* crystal by anomalous transmission [1, 2, 10], which introduces an angular offset of ~ 5 μrad from the reflected beam by the *C* crystal. The transmitted x-rays are finally reflected by the *S* crystal, which has the same Si(220) reflection and asymmetry angle as the *C* crystal, but canted by 5 μrad with respect to the *C* crystal to satisfy the Bragg condition. The narrow angular acceptance of the *S* crystal selects only a small portion of the transmitted fan from the *D* crystal, thereby reducing the energy width to sub-meV level to produce a highly monochromatized beam.

This is referred to as the CDTS (Collimation-Dispersion-Transmission-Selection) scheme following the optical path of the x-rays in the present paper. This is slightly different from the scheme used in Ref. [7], where the optical path is reversed. Our theoretical analysis and experimentation are based on the use of two identical CDTS units: one as monochromator, and the other as analyzer taking incident beam from the monochromator. The experiments were performed at beamline X16A of NSLS, where x-rays from a bending magnet source were preconditioned by a vertical collimating mirror, a Si(111) double-crystal monochromator and an exit slit before impinging onto the CDTS monochromator. The energy

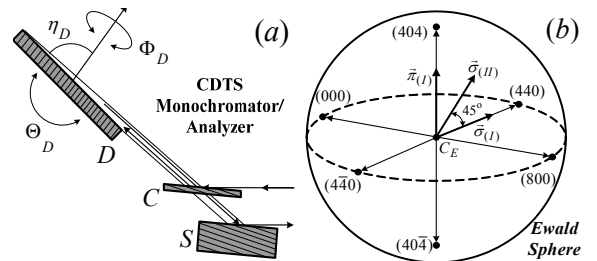


FIG. 1: Schematics of (a) the CDTS monochromator-analyzer scheme and (b) the 6-wave Si(000, 440, 440, 404, 404, 800) diffraction in the reciprocal space.

width of the incident x-rays was 2.5 eV at 9.1316 keV with the beam divergence set to $100\text{ (H)} \times 100\text{ (V)} \mu\text{rad}$ (horizontal \times vertical) and beam size to $2.5\text{ (H)} \times 0.5\text{ (V)} \text{ mm}^2$. The vertical beam size was chosen to fully illuminate the D crystal (200 mm in length) of the CDTS. The C and S crystals were constructed by a channel-cut crystal with a weak link in between for achieving the required detune angle of $5 \mu\text{rad}$. The theoretical analysis was carried out by numerical simulations within the framework of the dynamical theory of x-ray diffraction following a general algorithm developed and presented in Ref. [11], which includes the extreme case of MWD of exact backscattering at grazing incidence geometry of diffraction. The incident x-rays in the simulation were represented by the superposition of plane waves with a range of energies and incident directions that match those in the experiments.

For comparison and for understanding the main features, we first examine the angular and spectral behaviors of the CDTS scheme, treating the diffraction of the D crystal only in the two-wave approximation. In Ref. [7], tilting of the diffraction vector of the D crystal was considered only in the dispersion plane (DP). In Fig. 1 (a), such tilting angle for the CDTS scheme is denoted by Θ_D . However, the tilting angle Φ_D of the D crystal in the plane perpendicular to the DP is also important for the alignment of the diffraction vector relative to the DP. Such alignment is essential for the correct determination of the energy of the beam produced by the CDTS scheme. The development of the technique for eliminating the destructive contribution of MWD requires also the use of Φ_D .

Figure 2 shows the 2D (Θ_D, Φ_D) angular intensity distribution after the D reflection $I^{(2)}(\Theta_D, \Phi_D)$ (Fig. 2 (a)) and after the CDTS monochromator $I^{(4)}(\Theta_D, \Phi_D)$ (Fig. 2 (b)), calculated for the energy $E' \equiv E - E_{bs} = 0$ meV of exact backscattering. Here, the superscript “(i)” indicates the distribution after the (i)th reflection in the CDTS scheme; $E = hc/\lambda$; $E_{bs} = hc/\lambda_{bs}$, where $\lambda_{bs} = a\sqrt{1 - |\chi_0|}/4$ is the wavelength of exact backscattering, a is the lattice parameter of silicon, and χ_0 is the main Fourier component of crystal polarizability; h is the Planck constant and c is the speed of light in vacuum. The origin $(\Theta_D = 0, \Phi_D = 0)$ defines the normal incidence of x-rays with respect to the diffraction plane of the D crystal. The 2D intensity distribution $I^{(2)}(\Theta_D, \Phi_D)$ after the D reflection is nearly of concentric circular shape [1], with the angular width $\Delta\Theta_D^{(2)} \approx \Delta\Phi_D^{(2)} \approx 2\sqrt{|\chi_{800}|}$, where χ_{800} is the Fourier component of crystal polarizability for the (800) reflection. For the asymmetrical ($\eta_D > 0^\circ$) case, the angular position of the exact backscattering of the D crystal, as well as the angular peak position of the intensity distribution after the CDTS monochromator, which defines the monochromatization or transmission channel of x-rays in the 2D (Θ_D, Φ_D) phase space, is shifted in the DP by the value

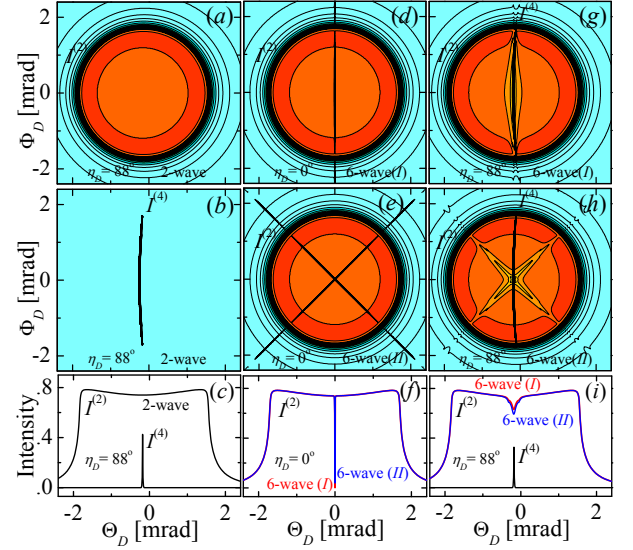


FIG. 2: (Color online). Intensity distribution of the CDTS scheme in 2D $I^{(i)}(\Theta_D, \Phi_D)$ (a-b, d-e and g-h) and 1D $I^{(i)}(\Theta_D, \Phi_D = 0)$ (c, f and i) after (i)th = 2nd (a, d-e and g-h) and (b) (i)th = 4th reflection calculated in two-wave (a-c) or multiple-wave (d-i) approximation for azimuthal orientation (I) (d and g) and (II) (e and h) of the D crystal surface with an asymmetry angle of $\eta_D = 88^\circ$ (a-c and g-i) or $\eta_D = 0^\circ$ (d-f). See text for further details.

$\Theta'_D(E' = 0) = -1/2|\chi_0|\tan\eta_D$ [2] relative to the symmetrical ($\eta_D = 0^\circ$) case. For an arbitrary energy E' of the incident x-rays this expression transforms to

$$\Theta'_D(E') = -[1/2|\chi_0| + E'/E_{bs}]\tan\eta_D. \quad (1)$$

The narrow angular width $\Delta\Theta_D^{(4)}$ of the intensity distribution $I^{(4)}(\Theta_D, \Phi_D)$ in the DP is determined by the acceptance angle $\Delta\theta_S \approx 5\mu\text{rad}$ of the S crystal of the CDTS scheme [2], whereas it is as broad as the (800) back reflection in the plane perpendicular to the DP, $\Delta\Phi_D^{(4)} \approx \Delta\Phi_D^{(2)}$.

Figure 3 shows the 2D energy-angular intensity distribution after the D reflection $I^{(2)}(E', \Phi_D)$ (Fig. 3 (a)) and of the CDTS scheme $I^{(4)}(E', \Phi_D)$ (Fig. 3 (b)) calculated at exact $\Theta'_D(E' = 0)$ angular position of the D crystal. The lines of equal intensity are parabolas $E'/E_{bs} = \Phi_D^2/2 + k$ with an arbitrary constant k . The energy width after the D reflection and after the CDTS monochromator at a fixed Φ_D position are given by $\Delta E^{(2)} \approx E_{bs}|\chi_{800}|$ and $\Delta E^{(4)} \approx E_{bs}\Delta\theta_S/\tan\eta_D$, respectively [1]. One can see that the relative energy resolution of the CDTS scheme $\Delta E^{(4)}/E_{bs}$ is determined essentially by the angular acceptance of the S crystal $\Delta\theta_S$ and the asymmetry angle η_D of the D crystal. With the present choice of the crystal parameters, we have $\Delta E^{(4)} \approx 1.6$ meV.

The parabola of maximum intensity of the CDTS monochromator moves along the E' axis for different Θ_D

value of the D crystal, and can be expressed, by taking into account Eq. (1), as

$$E'/E_{bs} = \Phi_D^2/2 - \Theta_D \cot \eta_D - 1/2|\chi_0|. \quad (2)$$

This expression defines the monochromatization channel of x-rays in the 3D (Θ_D, Φ_D, E') phase space of the CDTS scheme. Thus, the monochromatization of x-rays can be realized for any arbitrary Φ_D position of the D crystal. Clearly, according to Eq. (2), the energy E' of the exit beam from the monochromator is less sensitive to Φ_D than Θ_D . However, for the very high energy-resolution beam produced by the monochromator, even a small variation of Φ_D changes the energy E' significantly. Therefore, knowledge of Φ_D is important. Moreover, the fact that the monochromatization channel can be realized for any arbitrary Φ_D provides also the possibility to eliminate the destructive contribution from MWD as we will show below.

The Si(800) reflection in the backscattering condition is accompanied by the presence of 6-wave diffractions (000, 440, $\bar{4}\bar{4}0$, 404, $40\bar{4}$, 800) (see Fig. 1 (b)) [3, 4], which can be separated into two groups of 4-wave coplanar diffractions (000, 440, $\bar{4}\bar{4}0$, 800) and (000, 404, $40\bar{4}$, 800). Since the wavevectors of the $\langle 440 \rangle$ type reflections are normal to the wavevector of the incident beam, each of these groups of coplanar diffractions can be suppressed by appropriate choice of the polarization of the incident beam. We consider here two cases of the azimuthal orientation of the diffracting surface of the D crystal. These two cases are fundamentally different in terms of eliminating the destructive contribution of the MWD. Case (I): the surface normal \vec{n} of the diffracting surface of the D crystal located in the DP is defined by the [100] and [001] crystallographic axes, i.e., $\vec{n} = \cos \eta_D [100] + \sin \eta_D [001]$, of the D crystal. In this case, the [010] axis coincides with the polarization of the incident beam, labeled as $\vec{\sigma}_{(I)}$ in Fig. 1 (b). Case (II): the surface normal \vec{n} is defined by the [100] and $[0\bar{1}1]$ axes, i.e., $\vec{n} = \cos \eta_D [100] + \sqrt{2}/2 \sin \eta_D [0\bar{1}1]$. In this case, the $[011]$ axis coincides with the polarization of the incident beam, labeled as $\vec{\sigma}_{(II)}$ in Fig. 1 (b). For the $\vec{\sigma}_{(I)}$ polarization, only the (404) and ($40\bar{4}$) reflections can be excited and take part in the interaction

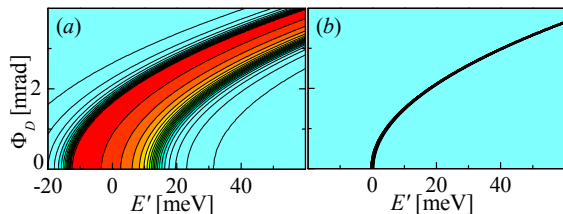


FIG. 3: (Color online). Intensity distributions $I^{(i)}(E', \Phi_D)$ of the CDTS scheme after $(i)^{th} = 2^{nd}$ (a) and $(i)^{th} = 4^{th}$ (b) reflection calculated in two-wave approximation.

with the backscattering (800) reflection. This results in a lower intensity region along the Φ_D axis in $I^{(2)}(\Theta_D, \Phi_D)$ of Fig. 2 (d) and (g). Similarly, only the (440) and ($\bar{4}\bar{4}0$) reflections can be excited with the $\vec{\pi}_{(I)}$ polarization. When the polarization of the incident beam differs from either the $\vec{\sigma}_{(I)}$ or $\vec{\pi}_{(I)}$, all $\langle 440 \rangle$ type reflections can be excited. The area of multiple-wave interaction (see Fig. 2 (e) and (h) for case (II) orientation of the D crystal) resembles a cross in $I^{(2)}(\Theta_D, \Phi_D)$ centered at $(\Theta_D = -1/2|\chi_0|\tan \eta_D; \Phi_D = 0)$. Fig. 2 (d-i) illustrates the two main properties of the multiple-wave interaction at exact backscattering with the introduction of the crystal surface asymmetry ($\eta_D \neq 0^\circ$). First, the area of the multiple-wave interaction becomes broader in the Θ_D direction with increasing asymmetry (larger η_D value). At $\eta_D = 0^\circ$, the width of the area at $\Phi_D = 0$ is about $10 \mu\text{rad}$ (Fig. 2 (d-f)), whereas it becomes $170 \mu\text{rad}$ for $\eta_D = 88^\circ$ (Fig. 2 (g-i)). Second, the loss of intensity as a result of MWD decreases with increasing η_D value. The loss of intensity is close to 100% for the symmetrical case ($\eta_D = 0^\circ$, Fig. 2 (f)) whereas it becomes about 30% for $\eta_D = 88^\circ$ (Fig. 2 (i)). These intensity losses and the regions of the multiple-wave interaction for the backscattering (800) reflection are in good agreement with the intensities and reflection regions of the individual $\langle 440 \rangle$ reflections. For all azimuthal orientations of the diffracting surface of the D crystal, the multiple-wave interaction region for case (II) has the narrowest width along the monochromatization channel in the Φ_D direction. Therefore, by introducing a small tilting from $\Phi_D = 0$ along the monochromatization channel, one can avoid the MWD and recover the intensity of the two-wave approximation (Fig. 2 (h)). The same however cannot be realized for case (I) where the multiple-wave interaction region extends across the entire monochromatization channel (Fig. 2 (g)). Therefore, for case (II), by tilting the D crystal in the Φ_D direction by several hundreds of μrad from the exact backscattering condition, destructive contribution from the MWD can be avoided.

Figure 4 (a-d) supports this conclusion. For both case (I) and (II), at $\Phi_D = 0$ mrad (Fig. 4 (a) and (c)), MWD reduces the intensity of the beam produced by the CDTS monochromator. In case (I), for an asymmetry angle $\eta_D = 88^\circ$, the loss of efficiency due to the presence of MWD varies from 10% to 30% within the reflection region. However, with $\Phi_D = 0.3$ mrad (Fig. 4 (b) and (d)), the intensity in case (II) recovers almost that of the two-wave approximation. Fig. 4 (c) and (d) also show that, although the MWD reduces the efficiency of the monochromator, there is no change to its energy and bandwidth in either cases. However, changing Φ_D from 0 to 0.3 mrad changes the energy of the CDTS by about 0.4 meV.

While MWD introduces a destructive contribution to the scattering intensity of x-ray backscattering optics, it can also have helpful practical applications. For exam-

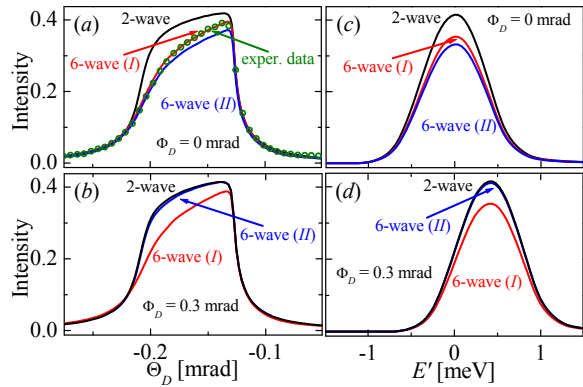


FIG. 4: (Color online) Angular $I^{(4)}(\Theta_D)$ (a and b) and spectral $I^{(4)}(E')$ (c and d) intensity distributions of the CDTS scheme calculated for $\Phi_D = 0$ mrad (a and c) and $\Phi_D = 0.3$ mrad (b and d). The conditions for the calculations are indicated for each curve. The green solid circles in (a) are experimental rocking curve measured with the D crystal surface in the (I) azimuthal orientation. The intensity was found to match the 6-wave (I) profile after background subtraction and re-scaling.

ple, although the detection of the x-ray back reflection is made difficult due to the coincidence of the incident and diffracted beams, we find that monitoring the $\langle 440 \rangle$ reflections, which is much easier, provides an efficient way to search for the $\langle 800 \rangle$ back reflection from the D crystal. Fig. 5 shows the behavior of the $\langle 440 \rangle$ reflection relative to the $\langle 800 \rangle$ reflection from the D crystal of the CDTS analyzer in the 2D (Θ_D, Φ_D) phase space obtained in our experiments and by numerical simulation. The D crystal is in case (I) azimuthal orientation. The experiment (Fig. 5 (a)) shows that the $\langle 440 \rangle$ reflection appears over a broad (Θ_D, Φ_D) region. As it approaches the transmission channel of the CDTS analyzer, the $\langle 440 \rangle$ reflection reduces in strength and eventually fades into the background where the Si(800) reflection appears. The measured distributions $I_{(440)}^{(2)}(\Theta_D, \Phi_D)$ of the $\langle 440 \rangle$ reflection and $I^{(4)}(\Theta_D, \Phi_D)$ of the CDTS analyzer compare well with the simulations (Fig. 5 (b)). Here, the transmission channel of x-rays from the CDTS analyzer can be expressed also by Eq. (2). This channel is parabolic in the (Θ_D, Φ_D) plane, with the vertex of the parabola located at $\Phi_D = 0$. The vertical feature located at $\Theta_D = 0$ in Fig. 5 is the symmetric $\langle 800 \rangle$ reflection from the front face of the D crystal. This transmission channel in the experiment is extremely important as it provides the reference for determining the energy produced by the CDTS monochromator. The distance in Θ_D between the symmetrical and asymmetrical channels, measured at $\Phi_D = 0$ in the experiment, gives the energy deviation of the incident beam from the backscattering energy of the CDTS analyzer at $E' = -5.77$ meV, which was used to generate the simulations shown in Fig. 5 (b). The ex-

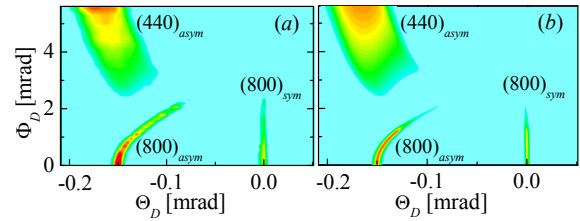


FIG. 5: (Color online). Experimental (a) and simulated (b) intensity distributions $I^{(i)}(\Theta_D, \Phi_D)$ of the CDTS analyzer. The D crystal diffracting surface was in case (I) azimuthal orientation. The simulations were performed in multiple-wave approximation for the $\langle 440 \rangle$ ($(i)^{th} = 2^{nd}$) and $\langle 800 \rangle$ ($(i)^{th} = 4^{th}$) asymmetrical ($\eta_D = 88^\circ$) and symmetrical ($\eta_D = 0^\circ$) reflections.

cellent agreement in Fig. 5 verifies the accuracy of the numerical simulations performed in the present paper.

For the practical applications of the CDTS scheme, the angular and spatial acceptance and the spectral efficiency are important performance parameters to consider. While the angular acceptance is determined essentially by the asymmetry of the C crystal as stated above, the spatial acceptance of the CDTS scheme is limited by the finite length of the D crystal and the asymmetry angle of the C and D crystals. The theoretical efficiency of the CDTS scheme is about 40%. Our detailed study to date indicates that the experimental efficiency essentially depends on the quality of the crystals and the diffraction surfaces. The improvement of these parameters allowed us to achieve an efficiency of about 18-20%.

We thank Yu. Shvyd'ko, A. Baron, M. Krisch, X.R. Huang, and Q. Shen for helpful discussions. Thanks are also due to Q. Shen for encouragement and support. This work and the operation of NSLS was supported by the U.S. Department of Energy, Office of Basic Energy Science, under Contract No. DE-AC02-98CH10886.

* E-mail: cai@bnl.gov

- [1] Yu. Shvyd'ko, X-Ray Optics: High-Energy-Resolution Application (Springer-Verlag, Berlin, 2004).
- [2] S.-L. Chang, X-ray Multiple-Wave Diffraction: Theory and Application (Springer-Verlag, Berlin, 2004).
- [3] A. Y. Nikulin *et al.*, Phys. Lett. A **319**, 434 (2003).
- [4] A. Souvorov *et al.*, Phys. Rev. B. **70**, 224109 (2004).
- [5] S.-L. Chang *et al.*, Phys. Rev. Lett. **94**, 174801 (2005).
- [6] S.-L. Chang *et al.*, Phys. Rev. B. **74**, 134111 (2006).
- [7] Yu. Shvyd'ko *et al.*, Phys. Rev. Lett. **97**, 235502 (2006).
- [8] R. Verbeni *et al.*, J. Sync. Rad. **3**, 62 (1996).
- [9] C. Masciovecchio *et al.*, Nucl. Instr. & Meth. B **111**, 181 (1996); *ibid.*, **117**, 339 (1996).
- [10] S. Kishino. J. Phys. Soc. Jap. **31**, 1168 (1971).
- [11] Yu. P. Stetsko and S.-L. Chang, Acta Crystallogr., Sect. A: Found. Crystallogr. **53**, 28 (1997).